The Astrophysical Journal, 728:102 (14pp), 2011 February 20 doi:10.1088/0004-637X/728/2/102
© 2011. The American Astronomical Society. All rights reserved. Printed in the U.S.A.

# THE DAWNING OF THE STREAM OF AQUARIUS IN RAVE

M. E. K. Williams[1], M. Steinmetz[1], S. Sharma[2], J. Bland-Hawthorn[3], R. S. de Jong[1], G. M. Seabroke[4], A. Helmi[5], K. C. Freeman[6], J. Binney[7], I. Minchev[1], O. Bienaymé[8], R. Campbell[9], J. P. Fulbright[10], B. K. Gibson[11], G. F. Gilmore[12], E. K. Grebel[13], U. Munari[14], J. F. Navarro[15], Q. A. Parker[3,16], W. Reid[16], A. Siebert[8], A. Siviero[1,14], F. G. Watson[3], R. F. G. Wyse[10], and T. Zwitter[17,18]

[1] Astrophysikalisches Institut Potsdam, An der Sterwarte 16, D-14482 Potsdam, Germany; mary@aip.de
[2] School of Physics, University of Sydney, NSW-2006, Australia
[3] Australian Astronomical Observatory, P.O. Box 296, Epping, NSW 1710, Australia
[4] Mullard Space Science Laboratory, University College London, Holmbury St Mary, Dorking, RH5 6NT, UK
[5] Kapteyn Astronomical Institute, University of Groningen, Postbus 800, 9700 AV Groningen, The Netherlands
[6] RSAA Australian National University, Mount Stromlo Observatory, Cotter Road, Weston Creek, Canberra, ACT 72611, Australia
[7] Rudolf Pierls Center for Theoretical Physics, University of Oxford, 1 Keble Road, Oxford OX1 3NP, UK
[8] Observatoire astronomique de Strasbourg, Université de Strasbourg, CNRS, UMR 7550, Strasbourg, France
[9] Department of Physics and Astronomy, Western Kentucky University, Bowling Green, Kentucky, USA
[10] Department of Physics and Astronomy, Johns Hopkins University, 3400 N Charles Street, Baltimore, MD 21218, USA
[11] Jeremiah Horrocks Institute for Astrophysics & Super-computing, University of Central Lancashire, Preston, UK
[12] Institute of Astronomy, University of Cambridge, Madingley Road, Cambridge CB3 0HA, UK
[13] Astronomisches Rechen-Institut, Zentrum für Astronomie der Universität Heidelberg, D-69120 Heidelberg, Germany
[14] INAF Osservatorio Astronomico di Padova, Via dell'Osservatorio 8, Asiago I-36012, Italy
[15] Department of Physics and Astronomy, University of Victoria, P.O. Box 3055, Station CSC, Victoria, BC V8W 3P6, Canada
[16] Department of Physics and Astronomy, Macquarie University, Sydney, NSW 2109, Australia
[17] Faculty of Mathematics and Physics, University of Ljubljana, Ljubljana, Slovenia
[18] Center of Excellence SPACE-SI, Ljubljana, Slovenia
*Received 2010 October 19; accepted 2010 December 8; published 2011 January 26*

## ABSTRACT

We identify a new, nearby (0.5 kpc $\lesssim d \lesssim$ 10 kpc) stream in data from the RAdial Velocity Experiment (RAVE). As the majority of stars in the stream lie in the constellation of Aquarius, we name it the Aquarius Stream. We identify 15 members of the stream lying between $30^\circ < l < 75^\circ$ and $-70^\circ < b < -50^\circ$, with heliocentric line-of-sight velocities $V_{\rm los} \sim -200\,{\rm km\,s^{-1}}$. The members are outliers in the radial velocity distribution, and the overdensity is statistically significant when compared to mock samples created with both the Besançon Galaxy model and newly developed code Galaxia. The metallicity distribution function and isochrone fit in the log $g$–$T_{\rm eff}$ plane suggest that the stream consists of a 10 Gyr old population with [M/H] $\sim -1.0$. We explore relations to other streams and substructures, finding that the stream cannot be identified with known structures: it is a new, nearby substructure in the Galaxy's halo. Using a simple dynamical model of a dissolving satellite galaxy, we account for the localization of the stream. We find that the stream is dynamically young and therefore likely the debris of a recently disrupted dwarf galaxy or globular cluster. The Aquarius stream is thus a specimen of ongoing hierarchical Galaxy formation, rare for being right in the solar suburb.

*Key words:* Galaxy: halo – Galaxy: kinematics and dynamics – solar neighborhood

*Online-only material:* color figures

## 1. INTRODUCTION

Under the current paradigm of galaxy formation, galaxies build via a hierarchical process and our Galaxy is deemed no exception. Relics of formation are observed as spatial and kinematic substructures in the Galaxy's stellar halo. Recent observations such as those from the Sloan Digital Sky Survey (SDSS) have brought a large increase in the detections of substructures within the outer reaches of the halo (out to $d < 80$ kpc). These streams have usually been detected as spatial overdensities from photometry (e.g., Yanny et al. 2000; Majewski et al. 2003; Belokurov et al. 2006; Newberg et al. 2009). Many of these structures have been identified as belonging to the debris of the Sagittarius dwarf spheroidal galaxy (Sgr dSph), which traces the polar orbit of this galaxy as it merges with the Milky Way. Furthermore, after subtracting such prominent substructures Bell et al. (2008) observed a dominant fraction of the halo to deviate from a smooth distribution, consistent with being primarily accretion debris.

Closer to the Sun, the spatial coherence of streams and substructures is not so easily discernible and most streams of stars are visible only as velocity structures, such as the Helmi et al. (1999) stream. Indeed, Helmi (2009) has shown that only at distances greater than ∼10 kpc do we expect that the structures associated with tidal debris to be observable as spatial overdensities. Therefore, if we wish to identify and study structures within the inner reaches of the halo—where they are most accessible for high-resolution follow-up observations—we must search utilizing kinematic data.

Kinematic surveys of the solar neighborhood are therefore ideal to detect substructures in the nearby regions of the Galaxy's halo. RAVE (RAdial Velocity Experiment) is an ambitious program to conduct a 17,000 square degree survey measuring line-of-sight velocities, stellar parameters, metallicities, and abundance ratios of up to 1 million stars (Steinmetz et al. 2006). RAVE utilizes the wide field (30 deg$^2$) multi-object spectrograph 6dF instrument on the 1.2 m UK Schmidt Telescope of the Anglo-Australian Observatory (AAO). RAVE's input catalogue

for the most part[19] has only a magnitude selection criterion of $9 < I < 13$, thus creating a sample with no kinematic biases. The observations are in the Ca-triplet spectral region at 840–875 nm with an effective resolution of $R = 7500$. Starting in 2003 April, at the end of 2010 RAVE had collected more than 465,000 spectra. RAVE's radial velocities are accurate to 1.3 km s$^{-1}$ when compared to external measurements, while the repeat observations exhibit an accuracy of 2 km s$^{-1}$ (Zwitter et al. 2008). These highly accurate radial velocities make RAVE ideal to search for kinematic substructures in an extended region around the sun. Indeed, with RAVE we now move away from studying the solar neighborhood (e.g., Nordström et al. 2004; $d < 0.2$ kpc) to examining the solar suburb ($d < 4$ kpc).

Using RAVE's highly accurate radial velocities, we have discovered a stream that lies mostly within the constellation of Aquarius at a distance of 0.5 kpc $\lesssim d \lesssim$ 10 kpc, in the direction $(l,\ b) \sim (55^\circ,\ -60^\circ)$ and at $V_{\rm los} = -200$ km s$^{-1}$. The velocity places the stream as part of the Galaxy's halo. As it lies in the direction of the constellation of Aquarius we have named it the Aquarius stream. The detection of this stream is described in Section 2. In Section 3, we compare the RAVE data to mock data from the Besançon Galaxy model and the newly developed galaxy modeling code Galaxia, which offers a number of significant advantages. Using these models we determine the significance of the detection and constrain its localization. In Section 4, we use RAVE's stellar parameters combined with Two Micron All Sky Survey (2MASS; *JHK*) photometry to infer basic properties of the stream population and derive distance estimates. We also use reduced proper motions (RPM) to obtain another estimate of the distances. The stream appears to be highly localized on the sky which is interesting considering the apparent proximity of the stream. In Section 5, we explore possible connections of the Aquarius stream to other known spatial and kinematic streams, finding that it is not linked to any previously reported structure. In Section 6, we investigate possible connections to other (marginal) overdensities in the RAVE data set and conclude that the stream is unlikely to be associated with any of them. A simple model of the recent disruption of a satellite in the Galaxy's potential is able to account for the observed localization. The Aquarius stream thus is a new and nearby enigma in the Milky Way's halo.

## 2. DETECTION IN RAVE

### 2.1. The Sample

RAVE measures the velocities of stars that are selected purely on the basis of their photometry, so it is free of kinematic biases. Over most of the sky the probability of a star's selection depends entirely on its apparent magnitude; only in directions toward the Galactic center is selection based on color as well as magnitude (DR1: Steinmetz et al. 2006; DR2: Zwitter et al. 2008). Furthermore, RAVE's radial velocities are accurate to $\leqslant$2 km s$^{-1}$ so fine substructures are best detected using radial velocities alone: combining them with proper motions and distances mean a significant loss of accuracy. The Aquarius stream was discovered in RAVE data as a structure seen in heliocentric radial velocity versus Galactic latitude/longitude space. When the stream was first noted, it was found to be most clearly defined by faint stars with low gravities, which suggests that the structure is at some distance from the Sun. Removing foreground giants enhances its visibility.

We use the internal release of RAVE from 2010 January that contains 332,747 observations of 252,790 individual stars. We use only those observations for which the signal-to-noise ratio (S/N) $> 13$ and the Tonry and Davis cross-correlation coefficient $R > 5$ to remove potentially erroneous observations. Note that, since not all observations have the more accurate signal-to-noise estimation, we use the S/N value which can underestimate the signal to noise (see DR2). For multiple observations of single stars the $V_{\rm los}$ were averaged, as were the stellar parameters for those observations that yielded an estimate of these parameters.

The Aquarius stream was found in the Galactic latitude slice $-70^\circ < b < -50^\circ$. As described above, it is also more marked for fainter stars. We therefore introduce an upper brightness limit to enhance the visibility of the stream. As noted in the first and second data release papers, a subset of the RAVE input catalog have *I* magnitudes from the SuperCOSMOS Sky Survey (Hambly 2001), which show an offset to DENIS *I* magnitudes. Not all RAVE stars have DENIS *I* magnitudes either. We therefore turned to 2MASS bands for our magnitude limit, even though this tends to bias against cool stars in our sample, and we potentially miss some candidates. We found that a limit of $J > 10.3$ produced the best differentiation of the stream from the background population, removing the brighter, nearby giants.

### 2.2. Detected Overdensity

Figure 1(a) shows the structure seen in heliocentric radial velocity, $V_{\rm los}$, against Galactic longitude, $l$, for the stars with the selection criteria $-70^\circ < b < -50^\circ$, $J > 10.3$. A clear structure begins at $V_{\rm los} \sim -150$ km s$^{-1}$ at $l = 30^\circ$ and extends down to $V_{\rm los} = -200$ km s$^{-1}$ at $l = 75^\circ$. This overdensity is particularly clear in Figure 1(b), where we plot the histogram for $V_{\rm los}$ in the region $-70^\circ < b < -50^\circ$, $J > 10.3$, $30^\circ < l < 75^\circ$. The stream can be seen as an excess of stars at negative velocities that is distinct from the general population.

We establish limits of $-250 < V_{\rm los} < -150$ km s$^{-1}$, $30^\circ < l < 75^\circ$, $J > 10.3$ to choose 15 candidates of the Aquarius stream, which are outlined by the red box in Figure 1 and listed in Table 1. Many stream candidates lack stellar parameter estimates, since they were observed early on by RAVE (DR1 does not include such estimates; see the data release papers for details). The average S/N is 20 for the stream candidates and one star (C2234420-082649) has a repeat observation, which is listed to show the consistency of the $V_{\rm los}$ results. As a double-check, the template fits to each of the spectra were eyeballed as were the zero-point fits (using sky radial velocities) for the fields the stars were observed in. No abnormalities were detected.

The RAVE internal release includes PPMX proper motions (Roeser et al. 2008). However, for our stream candidates we use in the following analysis PPMXL proper motions (Roeser et al. 2010), where the average proper motion error for the stream stars is reduced from $e_\mu = 6.8$ mas yr$^{-1}$ in PPMX to $e_\mu = 4.3$ mas yr$^{-1}$ in PPMXL. These proper motions are also listed in Table 1.

The average heliocentric radial velocity of the stream is $V_{\rm los} = -199 \pm 27$ km s$^{-1}$ and its Galactocentric radial velocity, i.e., the line-of-sight velocity in the Galactic rest frame (see Equation 10–8 of Binney & Tremaine 1998), is $V_{\rm gal} = -93 \pm 25$ km s$^{-1}$. When compared to $V_{\rm los} = -120 \pm 100$ km s$^{-1}$, $V_{\rm gal} = 0 \pm$

[19] Red giants in the direction of rotation were also targeted between $225^\circ < l < 315^\circ$, $5^\circ < |b| < 25^\circ$ with $J - K > 0.5$. This region is not discussed in this paper however.

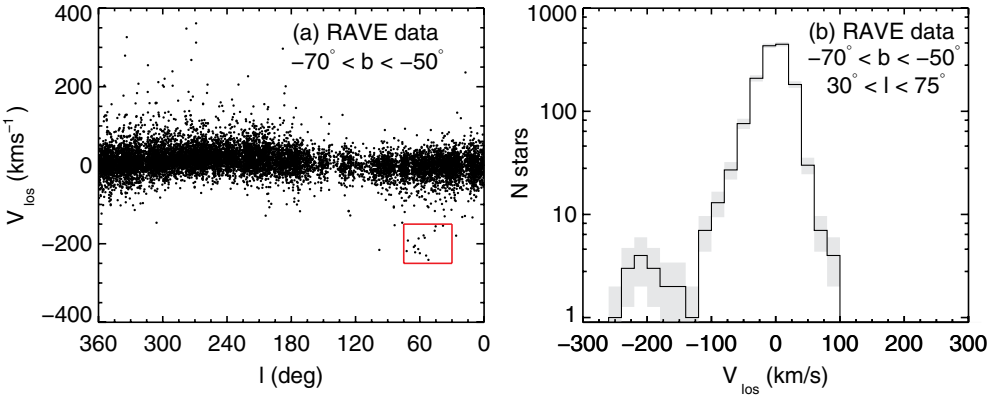


**Figure 1.** (a) $V_{\rm los}$ as a function of galactic latitude for RAVE data with $-70 < b < -50$, $J > 10.3$. The Aquarius Stream is identified as an overdensity of stars with $-250 < V_{\rm los} < -150\,{\rm km\,s^{-1}}$, $30^\circ < l < 75^\circ$, as delimited by the red box. (b) The histogram of $V_{\rm los}$ with the additional constraint $30^\circ < l < 75^\circ$ clearly shows the stream as an anomalous feature in the wings of the velocity distribution. The gray shading displays the $\pm 1\sigma$ limits.

(A color version of this figure is available in the online journal.)

**Table 1**
The Aquarius Stream Candidates Selected from the RAVE Data and Their Parameters

| ID | R.A. | Decl. | Obsdate | $V_{\rm los}$ (km s$^{-1}$) | e$V_{\rm los}$ (km s$^{-1}$) | $V_{\rm gal}$ (km s$^{-1}$) | $\mu_\alpha$ (mas yr$^{-1}$) | e$\mu_\alpha$ (mas yr$^{-1}$) | $\mu_\delta$ (mas yr$^{-1}$) | e$\mu_\delta$ (mas yr$^{-1}$) | S/N |
|---|---|---|---|---|---|---|---|---|---|---|---|
| J221821.2-183424 | $22^{\rm h}18^{\rm m}21\overset{\rm s}{.}20$ | $-18^\circ 20'64\overset{''}{.}5$ | 20060602 | −154.1 | 1.1 | −70.7 | −2.9 | 5.0 | −1.3 | 5.0 | 32.0 |
| C2222241-094912 | $22^{\rm h}22^{\rm m}24\overset{\rm s}{.}10$ | $-09^\circ 29'52\overset{''}{.}6$ | 20030617 | −241.0 | 2.6 | −127.6 | 32.9 | 4.0 | −55.2 | 4.0 | 18.8 |
| C2225316-145437 | $22^{\rm h}25^{\rm m}31\overset{\rm s}{.}70$ | $-14^\circ 32'77\overset{''}{.}9$ | 20040628 | −155.7 | 0.7 | −60.8 | −2.5 | 2.8 | −15.3 | 2.7 | 33.3 |
| C2233207-090021 | $22^{\rm h}33^{\rm m}20\overset{\rm s}{.}80$ | $-09^\circ 21'.4$ | 20030617 | −184.8 | 4.3 | −71.6 | 5.8 | 2.9 | −7.5 | 2.9 | 15.0 |
| C2234420-082649 | $22^{\rm h}34^{\rm m}42\overset{\rm s}{.}00$ | $-08^\circ 16'09\overset{''}{.}5$ | 20030618 | −177.1 | 1.4 | −62.4 | −1.0 | 2.1 | −25.2 | 2.1 | 25.3 |
| C2234420-082649 | $22^{\rm h}34^{\rm m}42\overset{\rm s}{.}00$ | $-08^\circ 16'09\overset{''}{.}5$ | 20050914 | −180.4 | 1.1 | −65.7 | −1.0 | 2.1 | −25.2 | 2.1 | 22.1 |
| J223504.3-152834 | $22^{\rm h}35^{\rm m}04\overset{\rm s}{.}40$ | $-15^\circ 17'14\overset{''}{.}9$ | 20060624 | −166.9 | 1.3 | −76.5 | 3.4 | 2.1 | −14.7 | 2.2 | 18.2 |
| C2238028-051612 | $22^{\rm h}38^{\rm m}02\overset{\rm s}{.}80$ | $-05^\circ 09'72\overset{''}{.}9$ | 20050807 | −213.6 | 1.6 | −89.4 | −2.3 | 4.0 | −7.4 | 4.0 | 14.8 |
| J223811.4-104126 | $22^{\rm h}38^{\rm m}11\overset{\rm s}{.}50$ | $-10^\circ 24'87\overset{''}{.}3$ | 20060804 | −230.1 | 1.9 | −123.9 | 28.5 | 2.7 | −2.0 | 2.7 | 22.3 |
| C2242408-024953 | $22^{\rm h}42^{\rm m}40\overset{\rm s}{.}80$ | $-02^\circ 29'93\overset{''}{.}9$ | 20050909 | −208.3 | 1.5 | −77.8 | 1.1 | 4.0 | −3.7 | 4.0 | 14.8 |
| C2246264-043107 | $22^{\rm h}46^{\rm m}26\overset{\rm s}{.}50$ | $-04^\circ 18'67\overset{''}{.}2$ | 20050807 | −205.0 | 1.7 | −81.0 | −10.6 | 2.5 | −19.3 | 2.5 | 20.5 |
| C2306265-085103 | $23^{\rm h}06^{\rm m}26\overset{\rm s}{.}60$ | $-08^\circ 30'63\overset{''}{.}8$ | 20030907 | −221.8 | 1.7 | −118.7 | 15.9 | 2.2 | −12.8 | 2.2 | 25.3 |
| C2309161-120812 | $23^{\rm h}09^{\rm m}16\overset{\rm s}{.}10$ | $-12^\circ 49'2\overset{''}{.}0$ | 20040627 | −224.1 | 2.1 | −133.1 | −25.3 | 2.1 | −99.5 | 2.1 | 14.6 |
| C2322499-135351 | $23^{\rm h}22^{\rm m}50\overset{\rm s}{.}00$ | $-13^\circ 32'31\overset{''}{.}5$ | 20040627 | −186.6 | 1.3 | −106.8 | −2.8 | 2.7 | −8.8 | 2.7 | 14.7 |
| J232320.8-080925 | $23^{\rm h}23^{\rm m}20\overset{\rm s}{.}90$ | $-08^\circ 56'6\overset{''}{.}1$ | 20060915 | −191.9 | 1.2 | −93.0 | 31.1 | 2.0 | −58.2 | 2.1 | 20.2 |
| J232619.4-080808 | $23^{\rm h}26^{\rm m}19\overset{\rm s}{.}50$ | $-08^\circ 48'8\overset{''}{.}7$ | 20060915 | −218.7 | 0.7 | −120.9 | 12.3 | 4.0 | −24.7 | 4.0 | 26.1 |

**Note.** The proper motions are from PPMXL.

$100\,{\rm km\,s^{-1}}$ for the halo and $V_{\rm los} = -30 \pm 45\,{\rm km\,s^{-1}}$, $V_{\rm gal} = 90 \pm 45\,{\rm km\,s^{-1}}$ for the thick disk at $(l, b) = (55^\circ, -60^\circ)$, this velocity indicates that the group to be a halo feature. However, it still has quite a large velocity even for the halo.

## 3. MODEL COMPARISONS

### 3.1. Besançon and Galaxia Models

To establish the statistical significance of the Aquarius overdensity we compare the RAVE sample to mock samples created using the Besançon Galaxy model (Robin et al. 2003) and the newly developed galaxy modeling code Galaxia (Sharma et al. 2011). Galaxia is based on the Besançon Galaxy model, but with several improvements. The first is a continuous distribution created across the sky instead of discrete sample points. Second is the ability to create samples over an angular area of arbitrary size. Third, it utilizes Padova (Girardi et al. 2002) isochrones which offer support for multiple photometric bands. Fourth, Galaxia offers greater flexibility with dust modeling. Once a data set without extinction has been created, multiple samples with different reddening normalization and modeling can be easily generated. Finally, with Galaxia multiple independent random samples can be generated, which is crucial for doing a proper statistical analysis. Due to the above mentioned advantages we chose Galaxia as our preferred model to create mock samples.

Table 2 lists the basic parameters for each of the two models. For the dust modeling, we chose the default value for the Besançon model, where the dust is modeled by an Einasto disk with a normalization of $A_V = 0.7$ mag kpc$^{-1}$. This is reasonable for the high latitudes that we simulate. Assuming an $R_V = 3.1$, this corresponds to a reddening rate of $E(B-V) = 0.23$ mag kpc$^{-1}$. No additional dust clouds were added. For the Galaxia model, we present results with the dust modeled by an exponential disk, with the reddening rate in the solar neighborhood normalized to 0.23 and 0.53 mag kpc$^{-1}$, where the latter is taken from Binney & Merrifield (1998). Also, we present results for a model where the reddening at infinity is matched to that of the value in Schlegel maps. To convert $E(B-V)$ to extinction in different photometric bands we used the conversion factors in Table 6 of Schlegel et al. (1998).

### 3.2. Mock Sample Generation

The mock samples were created from Galaxia and Besançon using analogous methodology. Firstly, to create the Besançon sample we queried $\Delta l \times \Delta b = 50^\circ \times 20^\circ$ regions using the

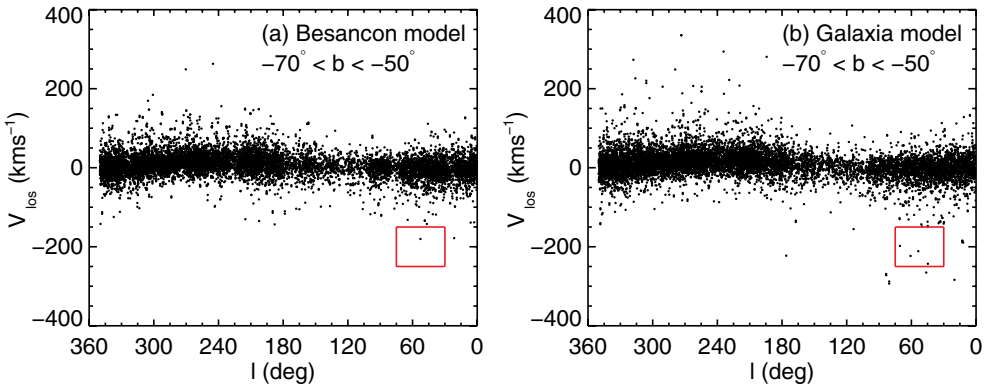


**Figure 2.** (a) The mock Besançon sample and (b) a mock Galaxia sample for $-70 < b < -50$, $J > 10.3$. As in Figure 1, the Aquarius stream region is delimited by the red box, with both mock samples displaying a paucity of stars in this region. A reddening rate of $E(B-V) = 0.23$ mag kpc$^{-1}$ is used for both the model samples displayed (see Section 3 for details).

(A color version of this figure is available in the online journal.)

**Table 2**
Parameters for the Galaxia and Besançon Models Used for Comparison with the RAVE Sample

| Model | Solar Position $(x,\ y,\ z)$ (kpc) | Solar Motion $(U,\ V,\ W)$ (km s$^{-1}$) | $V_c$ (km s$^{-1}$) | $E(B-V)$ Rate (mag kpc$^{-1}$) |
|---|---|---|---|---|
| Besançon | (−8.5, 0.0, 0.015) | (10.30, 6.30, 5.90) | 226.40 | 0.23 |
| Galaxia | (−8.0, 0.0, 0.015) | (11.10, 12.24, 7.25) | 226.84 | 0.23, 0.53, Schlegel |

online query form imposing the $I$-band magnitude limits of RAVE of $9 < I < 13$, making no biases in spectral type. A distance limit of $d = 20$ kpc is imposed as most RAVE stars (with the exception of a few notable Large Magellanic Cloud (LMC) stars—see Munari et al. 2009) should be within 15 kpc (Breddels et al. 2010). Grid-steps of 10° in $l$ and 5° in $b$ were used in the query.

To generate samples from Galaxia we simply generated a full catalog over the area specified by $0 < l < 360$, $-90 < b < 0$, and $9 < I < 13$ and then extracted the required samples from it after correcting for extinction. Since Galaxia allows oversampling, the initial catalog was generated with an oversampling factor of 10, so that later on 10 independent random realizations could be created.

Using Monte Carlo techniques each model was then resampled first to create a uniform distribution in $I$ magnitude and then resampled again to exactly mimic the shape of the DENIS $I$-band distribution in a $\Delta l \times \Delta b = 50^\circ \times 20^\circ$ region. This ensures that the distance distribution will be similar to the RAVE sample. Each generated sample is then further reduced to those stars with $J > 10.3$ to mimic our sample selection in Section 2. Finally, the number of stars in the mock sample is normalized to that of the RAVE sample in sub-regions of $\Delta l \times \Delta b = 25^\circ \times 10^\circ$, where this division into sub-regions was required to better suit the curved boundary of the RAVE survey area. For the Besançon sample, the $l$ and $b$ coordinates were smeared out to remove the discretization by adding a uniform randomization of the same extent (since the Galaxia sample was already smoothly distributed no such procedure was required). Also, for Galaxia ten mock data samples were created for each dust modeling scenario, enabling a better handle on the statistical significance of the Aquarius stream. Finally, to simulate the RAVE radial velocity measurement errors a scatter of $\sigma = 2$ km s$^{-1}$ was added to the models' radial velocities.

### 3.3. Statistical Significance of Aquarius

Figure 2 shows the Besançon and one of the Galaxia samples (with $E(B-V) = 0.23$ mag kpc$^{-1}$) for the same area of the sky as in Figure 1(a). We see that both models do a fair job of reproducing the gross features of the data. A detailed analysis of comparing both the Besançon and Galaxia models to RAVE will be presented in an upcoming paper by A. Ritter. In this analysis it is sufficient to note firstly that the Galaxia model produces a better representation of the density of halo stars (i.e., those stars with larger $V_{\rm los}$) than the Besançon model. Moreover, the Galaxia model better reproduces the $V_{\rm los}$ distribution as a function of Galactic latitudes than Besançon: for bins of 25° in Galactic latitude, on average Galaxia agrees with the data to within 2–3 km s$^{-1}$ for mean and dispersion in $V_{\rm los}$, respectively, compared to 3–4 km s$^{-1}$ for Besançon.

To compare the generated samples to the RAVE sample, we establish cells of size $\Delta l \times \Delta V_{\rm los}$ and for each cell compare the number of stars from RAVE and the mock samples. For each sample in the $i$th cell there are $N_i^{\rm Model}$ stars and we estimate the standard deviation by $\sigma_i = \sqrt{N_i^{\rm Model}}$. We consider an overdensity significant if

$$N_i^{\rm RAVE} - N_i^{\rm Model} > 4\sigma_i, \quad (1)$$

where $N_i^{\rm RAVE}$ are the number of RAVE stars in the $i$th cell and $N_i^{\rm Model}$ is either $N^{\rm Bes}$ or $N_i^{{\rm Gal},q}$, where $q = 1 \ldots 10$ in the latter signifies the sample number from Galaxia. Following a procedure similar to Helmi et al. (1999), we identify overdense regions in the Galactic latitude slice $-50 < b < -70$ by varying the cell sizes with longitude slices ranging from $\Delta l = 25,\ 35,\ 50,\ 70$ and radial velocity bins ranging from $\Delta V_{\rm los} = 20,\ 25,\ 35, \ldots,\ 100$. We then evaluate the percentage of the various cell sizes which identify the region around $30^\circ < l < 75^\circ$, $-250$ km s$^{-1}$ $< V_{\rm los} < -150$ km s$^{-1}$ as having a $4\sigma$ deviation. As we have 10 samples for Galaxia, we take the average over all the samples, obtaining a mean and standard deviation for this value.

The following results are found: using the Besançon model, 96% of the different cell sizes identify that the number of stars in the data are $4\sigma$ overdense around Aquarius compared to the model. For Galaxia using $E(B-V) = 0.23$ mag kpc$^{-1}$, we find

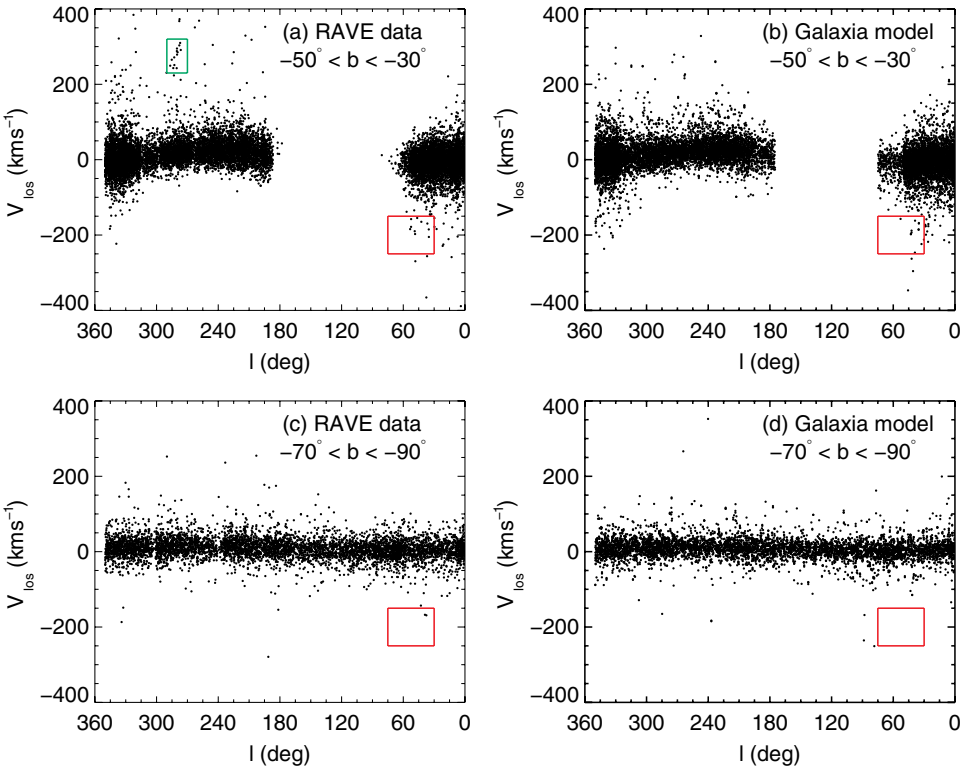


**Figure 3.** As in Figure 1 but for the latitude ranges $-50 < b < -30$ (a, b; top) and $-90 < b < -70$ (c, d; bottom) using the Galaxia model with Schlegel et al. (1998) dust mapping for comparison. LMC stars can be seen at $270^\circ < l < 290^\circ$, $230 < V_{\rm los} < 310\,{\rm km\,s^{-1}}$ in the RAVE data in the top panel and are outlined by the green box. The placement of the Aquarius stream from Figure 1 is outlined by the red box. Other than the LMC structures are not easily discernible.

(A color version of this figure is available in the online journal.)

that 80% ± 15% of cell sizes give Aquarius as a $4\sigma$ deviation, while $E(B-V) = 0.53$ mag kpc$^{-1}$ gives 75% ± 15% and the Schlegel results yield 80% ± 18%. How the dust is modeled at these high Galactic latitudes therefore has little impact on the results. In general we can conclude that the models robustly show that there is a statistically significant concentration of stars at the Aquarius stream's location. Indeed, for some cell sizes and models the overdensity can be as high as $11\sigma$. This confirms what can be seen by eye: the stream as an overdensity in the outlying regions of the velocity distribution.

### 3.4. Localization of the Stream

In addition to identifying the statistical significance of the Aquarius stream, we also used the models to search for additional members of the stream and possible related substructures. We compared the RAVE data and mock Galaxia samples for surrounding latitude cuts of $-50^\circ < b < -30^\circ$ and $-90^\circ < b < -70^\circ$, where once again we consider only those stars with $J > 10.3$. Figure 3 displays the data in these two latitude ranges compared to Galaxia models using the Schlegel dust model. We repeated the analysis of Section 3.3, looking for overdensities in the RAVE data compared to the Galaxia models, varying the cell size and identifying regions with repeated $4\sigma$ signals.

For the $-50^\circ < b < -30^\circ$ sample, the region around $270^\circ < l < 290^\circ$, $230\,{\rm km\,s^{-1}} < V_{\rm los} < 310\,{\rm km\,s^{-1}}$ is consistently identified for all the various dust models as significantly overdense: on average 95% of cell sizes identify this region as containing a $4\sigma$ signal. These stars are associated with the LMC and it is reassuring that our technique detects it.

For both latitude ranges, $-50^\circ < b < -30^\circ$ and $-90^\circ < b < -70^\circ$, there are no detections of statistically significant overdensities in the vicinity of the Aquarius stream's velocity and longitude range. Also, for the $-90^\circ < b < -70^\circ$ sample no particular region has consistent $4\sigma$ deviations when compared to the Galaxia models. The region around $-50^\circ < b < -30^\circ$, $320^\circ < l < 350^\circ$, $150\,{\rm km\,s^{-1}} < V_{\rm los} < 300\,{\rm km\,s^{-1}}$ is detected in ∼50% of the trials as being overdense for this latitude cut, irrespective of dust modeling. A similar detection is also found for the region $-70 < b < -50$, $260^\circ < l < 340^\circ$, $100\,{\rm km\,s^{-1}} < V_{\rm los} < 300\,{\rm km\,s^{-1}}$, in the same latitude range as the Aquarius stream. These detections are not as significant as Aquarius and are in a different region of the sky.

In general, we find that there are no stars clearly associated to the Aquarius stream in adjacent latitude cuts; no overdensities were detected in the vicinity of the stream's velocity and longitude. This may be caused in part by the survey boundary, but the sharp localization of the stream is nevertheless intriguing. In Section 6 we further investigate the localization of the Aquarius stream, examining its possible relation to the two marginal overdensities detected above.

## 4. POPULATION PROPERTIES OF THE AQUARIUS STREAM

### 4.1. Metallicity and $\log g$–$T_{\rm eff}$ Plane

RAVE gives estimates of stellar parameters from the spectra which we can use to establish the basic properties of the population of the Aquarius stream. Conservatively the stellar parameters are accurate to ∼0.2 dex in [M/H], 400 K in $T_{\rm eff}$ and 0.5 dex in $\log g$ when compared to external measurements, though internally the errors are significantly smaller (Zwitter et al. 2008). For 12 of the 15 stream candidates, we have estimates of stellar parameters.

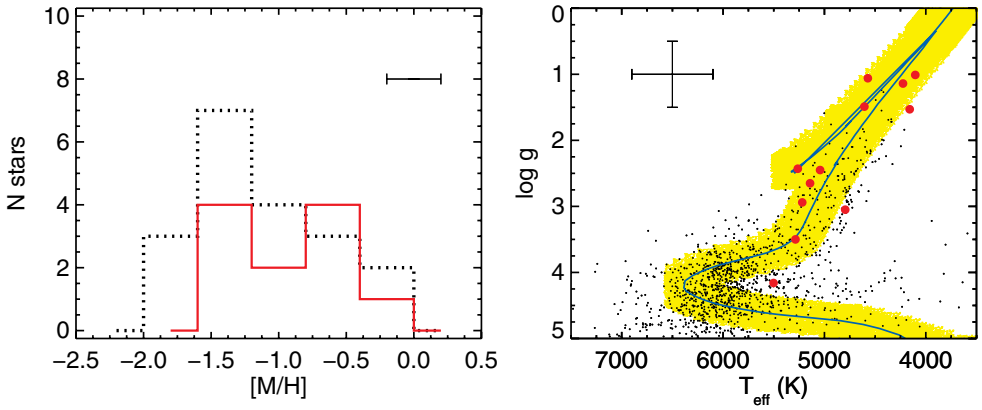


**Figure 4.** Left: MDF for the Aquarius stream members (red line), whose typical metallicity uncertainty is $\Delta([M/H]) \sim 0.2$ dex ($\pm 1\sigma$ shown). The MDF of other halo stars with $-70^\circ < b < -50^\circ$, $J > 10.3$, $|V_{los}| > 200\,km\,s^{-1}$ is shown for comparison (dotted line). Right: $T_{eff}$–log $g$ plane for RAVE stars in the region $-70^\circ < b < -50^\circ$, $30^\circ < l < 75^\circ$, $J > 10.3$. Stream candidates are highlighted as solid red points and a Padova isochrone with 10 Gyr, [M/H] $= -1$ overplotted. The yellow region indicates $1\sigma$ in both $T_{eff}$ and log $g$ from this isochrone.

(A color version of this figure is available in the online journal.)

Figure 4 shows the metallicity distribution function (MDF) and the log $g$–$T_{eff}$ plane of these stars where we compare the latter to the background population. The conservative estimates of the errors are also shown. Note that we do not apply the metallicity calibration of Equation 20 in Zwitter et al. (2008) as this calibration does not extend down to halo metallicities [M/H] $< -1.5$. Therefore, the derived MDF is best seen relative to background halo stars. We plot the MDF for stars selected $-70^\circ < b < -50^\circ$, $l \leqslant 30^\circ$ or $l \geqslant 75^\circ$, $J > 10.3$, $|V_{los}| > 200\,km\,s^{-1}$. The stream's MDF peaks at a slightly higher metallicity than these background halo stars with a slightly tighter distribution: the stream has an average [M/H] $= -1 \pm 0.4$ compared to [M/H] $= -1.1 \pm 0.6$ for the background. Both distributions show metallicities with are rather high for the halo. In the RAVE 3rd data release (Siebert 2011), it is shown that the metallicities are overestimated by the RAVE pipeline for stars with low S/N, an effect that would be on the order of 0.1 dex for the stream stars. This data release will present improved stellar parameters from a modified pipeline, as well as a new metallicity calibration from an extended metallicity range. Hence, these results should a better handle on the stream's MDF. Clearly, however, follow-up high-resolution spectroscopy is required to derive accurate abundances to better understand the group's chemical abundance properties. Nevertheless, from the initial RAVE metallicities, we can conclude that the stream's MDF is consistent with background halo stars.

Using Padova isochrones (Girardi et al. 2002) we find the best-fitting isochrone to be that of 10 Gyr, [M/H] $= -1$ which is overplotted in Figure 4 (right), as well as a highlighted region showing the $\pm 1\sigma$ bounds in (log $g$, $T_{eff}$) from this curve. Most of the stream stars fall within this region, though clearly the isochrone fit is preliminary given the size of the stellar parameter errors. From both the MDF and the isochrone fit, however, there is a general indication that the Aquarius stream is metal-poor and old.

### 4.2. Isochrone-derived Distances

We use the isochrone fit from above to derive distances to the candidate stars, using the $J$-band magnitude. To derive $M_J$ from the isochrone we find the nearest point along the isochrone to the actual data point by minimizing the distance in log $g$ and $T_{eff}$ between them, normalized by the standard error in each. Extinction is of the order of $A_J = 0.04 \pm 0.01$, and is calculated iteratively from the distances using Schlegel et al. (1998) dust maps and assuming a Galactic dust distribution as in Beers et al. (2000). Errors are calculated via Monte Carlo, generating 100 points around the data point with $\sigma_{T_{eff}} = 400$ K and $\sigma_{\log g} = 0.5$ dex, propagating through to a distribution of distances, from which a standard deviation is derived.

The distances are listed in Table 3 as $d_I$, where the distances range from 0.4 to 9.4 kpc (distance moduli: $m - M = 8.3$ to $m - M = 14.9$), with a mean distance of $d_{av} = 3.8 \pm 3.2$ kpc ($m - M = 12.9$). There is a hint of a bimodal population of closer (sub- and red clump giants) and farther stars (tip of the giant branch). However, given the uncertainties in the stellar parameters these distances are uncertain and the reality of this bimodality is therefore debatable; in the next section we develop another distance estimate which has a smoother distribution function.

The large distance range raises the question whether the Aquarius stream is a distinct entity or comprised of multiple structures. The high-resolution abundances mentioned above would help answer this question by ascertaining if the group has any distinctive chemical signatures compared to other halo stars. Occam's razor would weigh against two structures forming this localized stream however. Further, in Section 6.1 we develop a model for the Aquarius stream under the assumption of a single satellite dissolving in the Galaxy's potential. The model predicts that the stream is spread in $XYZ$ away from the sun, with distance $d_{model} = 3.2 \pm 0.8$ kpc in the direction $30^\circ < l < 75^\circ$, $-70^\circ < b < -50^\circ$. The distance range derived above therefore probably reflects more on the distance errors than the real distribution for the stream. We assume that the Aquarius stream is a single, distinct object.

The isochrone from Figure 4 has an $I$-band turnoff of $M_I = 3.5$. Hence, for the distance moduli above we could expect turnoff stars in the range $I = 11.8$–$18.5$. The lower magnitude falls within the RAVE magnitude limits ($9 < I < 13$). However, RAVE's unbiased selection criteria mean that the thin disk dominates dwarf/turnoff stars, even at these higher magnitudes. Our sample of halo dwarfs is therefore too small to detect the turnoff, and we only see giant stars in our Aquarius stream sample from RAVE.

**Table 3**
The Aquarius Stream Candidates Selected from the RAVE Data and Their Parameters

| ID | Obsdate | $J$ | $K$ | $T_{\rm eff}$ (K) | [M/H] | $\log g$ | $d_{\rm I}$ (kpc) | $d_{\rm R}$ (kpc) | $d_{\rm B}$ (kpc) | $d_{\rm Z}$ (kpc) | $d_{\rm BB}$ (kpc) |
|---|---|---|---|---|---|---|---|---|---|---|---|
| J221821.2-183424 | 20060602 | 10.34 | 9.68 | 4572 | −1.54 | 1.06 | 5.6 ± 2.1 | 2.4 ± 1.0 | 9.6 ± 2.1 | 6.7 ± 2.9 | 2.8 ± 0.5 |
| C2222241-094912 | 20030617 | 10.64 | 9.79 | ··· | ··· | ··· | ··· | 16.3 ± 11.9 | ··· | ··· | ··· |
| C2225316-145437 | 20040628 | 10.34 | 9.57 | 4104 | −1.29 | 1.01 | 7.3 ± 2.7 | 3.4 ± 1.5 | 10.3 ± 2.4 | 7.9 ± 3.1 | 1.4 ± 0.1 |
| C2233207-090021 | 20030617 | 11.66 | 11.28 | ··· | ··· | ··· | ··· | 0.8 ± 0.3 | ··· | ··· | ··· |
| C2234420-082649 | 20050914 | 10.67 | 10.13 | 5263 | −2.02 | 2.43 | 1.9 ± 0.7 | 1.9 ± 0.8 | ··· | 3.1 ± 2.8 | ··· |
| J223504.3-152834 | 20060624 | 10.36 | 9.65 | 4795 | −0.33 | 3.05 | 1.0 ± 0.5 | 2.5 ± 1.1 | ··· | 1.3 ± 1.0 | ··· |
| C2238028-051612 | 20050807 | 11.53 | 10.74 | 4606 | −0.86 | 1.49 | 7.1 ± 2.7 | 6.7 ± 5.4 | ··· | ··· | ··· |
| J223811.4-104126 | 20060804 | 10.42 | 9.90 | 5502 | −0.78 | 4.16 | 0.4 ± 0.1 | 0.5 ± 0.2 | 0.3 ± 0.1 | 0.5 ± 0.9 | 0.4 ± 0.3 |
| C2242408-024953 | 20050909 | 11.63 | 10.82 | 4159 | −0.75 | 1.53 | 9.4 ± 3.4 | 13.4 ± 8.7 | ··· | 8.5 ± 5.6 | ··· |
| C2246264-043107 | 20050807 | 11.26 | 10.72 | 5142 | −1.22 | 2.65 | 1.8 ± 0.9 | 1.8 ± 0.7 | 3.9 ± 2.1 | 3.2 ± 3.0 | 2.0 ± 0.8 |
| C2306265-085103 | 20030907 | 10.31 | 9.47 | ··· | ··· | ··· | ··· | 3.3 ± 1.5 | ··· | ··· | ··· |
| C2309161-120812 | 20040627 | 10.68 | 9.97 | 5219 | −0.66 | 2.94 | 1.0 ± 0.6 | 5.5 ± 2.9 | ··· | 1.5 ± 1.4 | ··· |
| C2322499-135351 | 20040627 | 10.82 | 10.28 | 5043 | −0.64 | 2.45 | 1.9 ± 0.9 | 2.1 ± 0.8 | ··· | 2.3 ± 1.6 | ··· |
| J232320.8-080925 | 20060915 | 10.96 | 10.47 | 5286 | −1.10 | 3.50 | 0.7 ± 0.4 | 0.8 ± 0.3 | 1.0 ± 0.5 | 1.8 ± 2.2 | 1.1 ± 0.7 |
| J232619.4-080808 | 20060915 | 10.51 | 9.76 | 4225 | −1.22 | 1.14 | 6.7 ± 2.7 | 5.6 ± 2.9 | 10.6 ± 2.8 | 7.1 ± 3.0 | 3.5 ± 0.6 |

**Notes.** The distances $d_{\rm I}$ are derived from the isochrone in Figure 4 while $d_{\rm R}$ are derived in Section 4.3. The extra distances are $d_{\rm B}$ (Breddels et al. 2010), $d_{\rm Z}$ (Zwitter et al. 2010), and $d_{\rm BB}$ (Burnett & Binney 2010).

### 4.3. Reduced Proper Motion Diagram

The coherence of the group selection is shown by the reduced proper motion diagram (RPMD), which plots the RPM against color. Described in detail in Seabroke et al. (2008), the RPMD essentially creates an HR diagram from the proper motions, where the absolute magnitude is smeared by the variation in the tangential speed of the stars. Halo stars have a large dispersion in tangential velocity and so this smearing is large. In contrast, for a small, nearby section of a stream the transverse velocity spread is small and we effectively recover magnitudes for the stars. The RPM is given by

$$H_J = J + 5\log\mu + 5 = M_J + 5\log v_{\rm T} - 3.379, \qquad (2)$$

where $J$ and $M_J$ are the apparent and absolute magnitudes, respectively, $\mu$ is the proper motion in arcsec yr$^{-1}$, and $v_T$ is the tangential velocity in km s$^{-1}$. Here we have again used 2MASS colors. Thus, from the observables $J$ and $\mu$ we can establish something about the more fundamental parameters $M_J$ and $v_{\rm T}$ without requiring either a distance or a radial velocity. Figure 5 gives the RPMD for the stars in our magnitude and latitude selected sample with the Aquarius stream candidates overplotted, where for the latter the more accurate PPMXL proper motions were used. Note that for the distances of these stars the reddening will also be of the order of $E(J-K) \sim 0.02$, which does not effect the plot significantly and is neglected. The isochrone from Figure 4 is overplotted, where we find that a large tangential velocity of $v_T = 150$–$350$ km s$^{-1}$ is required to shift the isochrone to a reasonable fit, which compares to $v_T \sim 230 \pm 100$ km s$^{-1}$ for the halo for $(l, b) = (55°, -60°)$. Once again, the group is consistent with a halo stream.

We will see in Section 6 that the tangential velocity for the stream is indeed within a relatively narrow range as shown in Figure 5. A few of the redder, more-distant giants deviate from the rest of the group but they also have larger errors in their proper motions, which translates into larger RPM errors as shown: they are within $2\sigma$ of the group fit. The consistency of the fit for the bluer (nearer) stars supports their inclusion in the candidate list, though the range in values for the RPM of halo stars means that we cannot exclude contamination from the halo. Indeed, from Figure 1 it is clear that we expect a few of the stars

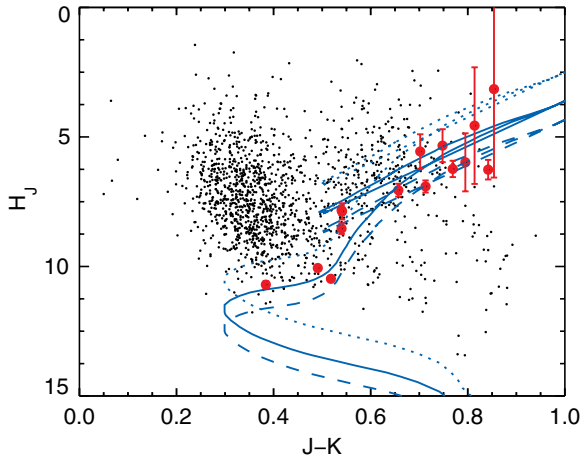


**Figure 5.** Reduced proper motion diagram for the background RAVE stars (black points) and the Aquarius stream stars (red points). The isochrone from Figure 4 is plotted with a tangential velocity of $v_T = 250$ km s$^{-1}$ (solid line), $v_T = 150$ km s$^{-1}$ (dotted line), and $v_T = 350$ km s$^{-1}$ (dashed line). The coherency of the group is clear also in this diagram.
(A color version of this figure is available in the online journal.)

to be non-members. We therefore take the consistency of the RPMD to be a good indication of the consistency of the Aquarius member selection but not absolute proof of membership.

### 4.4. RPM-derived Distances

If we accept the group's tangential velocity of $v_T = 250$ km s$^{-1}$, we can use the RPM to establish a second estimate of the distance to the stars. From Equation 2 we have the distance modulus,

$$J - M_J = J - H_J + 5\log v_{\rm T} - 3.379. \qquad (3)$$

From this we have distance moduli ranging from 8.5 to 16 for the group members. The corresponding distances are listed in Table 3 as $d_{\rm R}$, with the errors calculated using the upper and lower tangential velocity bounds as well as the proper motion errors in $H_J$. These distances differ somewhat from those calculated using the isochrones in Section 4.2 but are